# Wavelength scaling of photoionization circular dichroism of atomic electron ring currents and its effect on photoelectron spin polarization

Meng Han [1,2] Peipei Ge,[1] Yiqi Fang,[1] and Yunquan Liu [1,3,4,*]

[1]*State Key Laboratory for Mesoscopic Physics and Collaborative Innovation Center of Quantum Matter,*
*School of Physics, Peking University, Beijing 100871, China*
[2]*Laboratorium für Physikalische Chemie, ETH Zürich, Zurich 8093, Switzerland*
[3]*Collaborative Innovation Center of Extreme Optics, Shanxi University, Taiyuan, Shanxi 030006, China*
[4]*Beijing Academy of Quantum Information Sciences, Beijing 100193, China*

Circularly polarized orbitals in atoms are referred to as electron ring currents with a helical angular phase and thus manifest circular dichroism in photoionization by circularly polarized light fields. Opposite circular dichroism has been revealed in single-photon and nonadiabatic tunneling ionization regimes. The transition of the circular dichroism and its underlying mechanism are still not clear. Here, we systematically study the wavelength scaling of photoionization circular dichroism of electron ring currents. We present a universal description of the dichroic photoelectron energy spectra and the spin polarization from the infrared to the extreme ultraviolet regions. We reveal that the channel interference and competition via the intermediate states with different angular quantum numbers in a few-photon ionization regime give rise to the transition of the circular dichroism and the spin polarization of photoelectrons.

## I. INTRODUCTION

Circular dichroism refers to the different response of a physical system to the change of the helicity of an incoming circularly polarized light [1,2]. The emergence of circular dichroism indicates that the system possesses chiral properties, such as the chiral structure for chiral molecules. Since the chiral objects or systems exist widely in nature, circular dichroism has attracted much attention ranging from physics [3–5] to stereochemistry [6] and life sciences [7]. As a fundamental chiral object, atomic electron ring currents are electronic states or orbitals $|l, m\rangle = Y_{lm}(\theta, \phi)$ with nonzero $m$ [8], where $Y_{lm}$ is the spherical harmonic with an angular quantum number $l$ ($l > 0$) and magnetic quantum number $m$ ($0 < |m| \leqslant l$). Electron ring currents carry an angular phase $e^{im\phi}$ with respect to the azimuthal angle $\phi$, classically corresponding to the clockwise ($m > 0$) or anticlockwise ($m < 0$) rotation around the quantization axis. Due to the helicity of the angular phase $e^{im\phi}$, the electron ring current has an intrinsic chirality and would be expected to manifest circular dichroism in photoionization.

The study of photoionization circular dichroism in single- and few-photon ionization can be traced back to the 1960s and 1970s [9–11]. There, scientists extensively studied the photoionization of alkali atoms, whose ground state is the $s$ orbital without any ring currents. Note that the Fano and Bethe propensity rule in single-photon ionization can be traced back to the different magnitudes of the Wigner-$3j$ symbols for different $l, m$ combinations [12]. In the 1990s, the photoionization circular dichroism of circular Rydberg wave packets attracted much attention [13,14]. In the past

10 years, the photoionization circular dichroism of rare-gas atoms by multiphoton ionization or tunneling ionization has attracted considerable attention [15–20], such as experimental efforts on the outermost $p$ shell of argon atoms [18–21], due to the promising potential of generating spin-polarized photoelectrons [22–27]. The photoionization circular dichroism of ring-current orbitals, as a basic chiral interaction between rotating lights and electrons, is fundamentally important in both science and applications [28–36]. However, it is less explored in single- and few-photon ionizations [3,36–38]. Recently, the polarization control of XUV free-electron lasers has been realized [39]. On the other hand, the tabletop production of circularly polarized ultraviolet high-order harmonics has been recently demonstrated with counter-rotating circularly polarized driving fields [40–47]. Therefore, the ultrafast circular dichroism and photoelectron spin polarization from ring currents in single- or few-photon ionization regimes would be theoretically and experimentally interesting in the future for providing highly spin-polarized electron sources. To this end, the universal description for this chiral ionization interaction and its effect on photoelectron spin polarization is an important central topic in ultrafast science.

In this paper, we theoretically investigate the wavelength scaling of photoionization circular dichroism of the ground-state ring-current orbitals [$p_+$ ($m = 1$) and $p_-$ ($m = -1$)] of argon atoms from nonadiabatic tunneling ionization to single-photon ionization. Using the *ab initio* solution of the three-dimensional time-dependent Schrödinger equation (TDSE) and the simulation with the strong-field approximation (SFA), we calculate the photon-frequency-dependent ionization probabilities and photoelectron energy spectra from the corotating orbital ($p_+$) and the counter-rotating orbital ($p_-$) in a right circularly polarized light field. By comparing with the benchmark results of TDSE, we show that the SFA fails to

*yunquan.liu@pku.edu.cn

describe the circular dichroism in few-photon ionization due to the lack of intermediate states. Based on a state-resolved calculation and analysis, we identify that the quantum interference and competition of the ionization channels via the intermediate states with different angular quantum numbers give rise to the transition of the circular dichroism and the photoelectron spin polarization in a two-photon ionization regime.

## II. METHOD

We study the photoionization of the $3p$ state that is obtained in an effective potential $V_{eff} = -[Z + (Z_{full} - Z)e^{-r/r_s}]/r$ as the ground state of argon atoms by numerically solving the three-dimensional TDSE [48,49]. Here, $Z = 1$ and $Z_{full} = 18$ are the asymptotic ion charges as $r \to \infty$ and $r \to 0$, respectively, and a screening length $r_s = 0.21494$ is tuned to match the ionization potential $I_p = 0.579$ a.u. for argon atoms (only for the $j = 1/2$ ion channel). We used up to 50 angular momenta and the radial grid step size is 0.01 a.u. The TDSE is solved using the Crank-Nicolson propagator in the time axis with a step size of $10^{-3}$ a.u. The wave function is spatially expanded with spherical harmonics, so that the populations of the states $|l, m\rangle$ can be monitored in real time. In SFA, the transition-matrix element is given by $M_p = -i \int dt \langle \psi_v(\boldsymbol{p}, t) | \boldsymbol{r} \cdot \boldsymbol{E}(t) | \psi_0 \rangle$ [50], where $|\psi_0\rangle$ is the ground state obtained using the imaginary-time propagation method in the effective potential and $|\psi_v(\boldsymbol{p}, t)\rangle$ is the Volkov state with the photoelectron final momentum $\boldsymbol{p}$. Intrinsically, the SFA ignores intermediate states in the interaction. In the calculations, we used a right circularly polarized laser pulse with a 12-cycle sine-square envelope at an intensity of $1.0 \times 10^{13}$ W/cm$^2$ (electric field $E \approx 0.01689$ a.u.), and the sense of rotation of the electron orbital is determined by $m = 1$ (corotating) and $m = -1$ (counter-rotating). The light frequency was continuously varied from 0.05 a.u. (1.35 eV) to 2.0 a.u. (54.4 eV) with a step size of 0.005 a.u.

## III. RESULTS AND DISCUSSION

We first compare the photoionization circular dichroism of electron ring currents in the single-photon (at 45.6 nm) and nonadiabatic tunneling (at 800 nm) ionization regimes in Fig. 1. In single-photon ionization, the photoelectron energy spectrum manifests as a single peak and the ionization probability of the corotating ring current is about four times as much as that of the counter-rotating ring current, indicating that the corotating orbital with respect to the XUV light will be preferentially ionized. This can be understood by a classical picture that the effective interaction time between the light and electron is much longer when they are corotating. In tunneling ionization, the circular dichroism is surprisingly reversed. The circularly polarized IR light field prefers to tunnel ionize the counter-rotating ring current, which can be explained by the nonadiabaticity of light-induced tunneling [51] or simply the blueshift of photons in the counter-rotating case [21].

From the two extreme cases, one can note that the photoionization circular dichroism of the electron ring currents has a remarkable dependence on the light frequency. The frequency dependence is not trivial and it reflects the rich
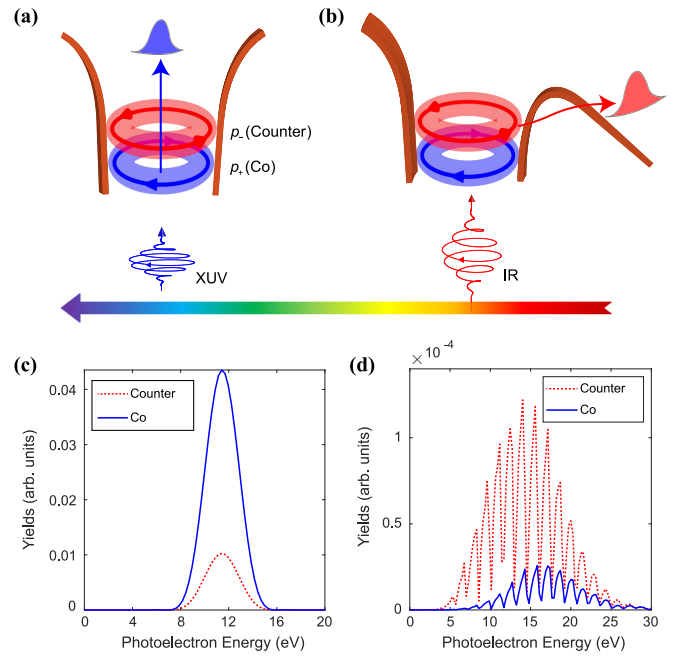


FIG. 1. (a), (b) Schematic representation of the photoionization circular dichroism of electron ring currents [$p_+$ (blue) and $p_-$ (red dashed)] in a right circularly polarized light field in the single-photon ionization and nonadiabatic tunneling ionization regimes, respectively. The $p_+$ and $p_-$ orbitals are energy degenerated and their separation in the figure is for clarity. (c), (d) The calculated photoelectron energy spectra from the two orbitals with the TDSE method at a light angular frequency of 1.0 a.u. (45.6 nm) and 0.057 a.u. (800 nm), corresponding to single-photon ionization and nonadiabatic tunneling ionization, respectively.

electron dynamics in this chiral interaction. The rotation angular frequency of the ring currents can be estimated as $\omega_0 = m\hbar/(m_e r^2)$, where $r$ is the most probable orbit radius and $m_e$ is the electron mass. For the ground-state ring currents in typical rare-gas atoms, the magnetic quantum number is $m = \pm 1$ and the orbit radius is $r \approx 1.0$ a.u., and thus the angular frequency of ring currents is much faster than that of the widely used Ti:sapphire laser at a center wavelength of 800 nm ($\omega_L = 0.057$ a.u.). Thus, in multiphoton or tunneling ionization the rotating electron ring current can be viewed as a spatially continuous and uniform distribution by the incoming IR photons, so that the relative rotation phases between them is not important. For the single-photon ionization case, the light wavelength is in the extreme ultraviolet regime, and the angular frequency of the light field becomes larger than that of the electron ring currents. The assumption of spatial continuity of the electron orbital will be therefore broken. In the gap between the two regimes, their angular frequencies are comparable, and thus the phase matching between the light and orbital will become very important and the electron dynamics should be very rich and complex. Therefore, the scaling law of the photoionization circular dichroism of electron ring currents with respect to the light frequency is fundamentally essential. Especially, it is interesting to investigate the underlying mechanism of the transition of the circular dichroism.
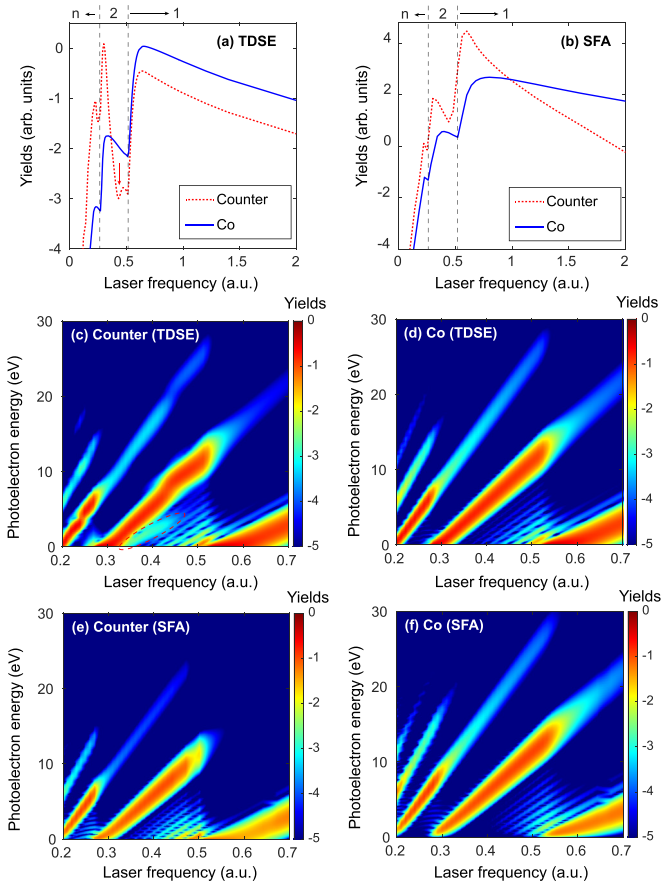
FIG. 2. (a), (b) Frequency-dependent photoelectron yields from $p_+$ (corotating) and $p_-$ (counter-rotating) orbitals in a right circularly polarized laser field calculated with the TDSE and SFA model, respectively. The vertical dashed lines indicate the critical frequencies from multiphoton ionization to single-photon ionization. The red arrow in (a) indicates the rapid decrease of the yield in the counter-rotating geometry. (c), (d) Frequency-dependent photoelectron energy spectra by solving the TDSE for the counter-rotating and corotating orbitals, respectively. In (c), the red dashed ellipse highlights the subpeak splitting from the main ATI peak in the two-photon ionization regime. (e), (f) The photoelectron energy spectra using the SFA model. The spectra (c)–(f) are normalized by the maximum yield at each laser frequency. In all panels, the photoelectron yields are in a logarithmic scale.

In Figs. 2(a) and 2(b), we illustrate the angle- and energy-integrated ionization probabilities from the two orbitals as a function of the photon frequency using the TDSE and SFA models, respectively. Generally, the ionization probabilities increase with respect to the photon frequency. One can note that a typical ladder-shaped structure appears when the photon frequency satisfies $\omega_L = I_p/n$, where $n$ is the number of photons required in photoionization. Both models reveal that the ionization probability of the counter-rotating geometry is larger than that of the corotating geometry in a multiphoton regime ($\omega_L < 0.25$ a.u.). As seen in Fig. 2(b) for the SFA results, the probability of the counter-rotating geometry is always larger than that of the corotating geometry until entering in the deep single-photon ionization regime when $\omega_L > 1.0$ a.u. Afterwards, the probability of corotating geometry

will be much larger than that of counter-rotating geometry. However, strikingly, the accurate TDSE result shows that the ionization probability of the counter-rotating geometry drops sharply in the two-photon ionization regime, as indicated by the red arrow in Fig. 2(a). When the frequency continues to increase into the single-photon ionization regime ($\omega_L > I_p$), the TDSE result shows that the ionization probability of the corotating geometry then becomes larger than that of the counter-rotating geometry. In Fig. 2(b), there is no such sudden decrease for the ionization probability of the counter-rotating geometry in a two-photon regime. The less accurate behavior of SFA can be attributed to the neglect of the intermediate states, as well as the Coulomb potential. The transition of circular dichroism in the two-photon ionization regime is particularly interesting, which the SFA model cannot capture.

We further show the photon-frequency-dependent photoelectron energy spectra of the co- and counter-rotating geometries using the TDSE and SFA models in Figs. 2(c)–2(f), respectively. The energy of each order above-threshold ionization (ATI) peak [52] increases linearly with respect to the photon frequency, and the channel closing and channel shifting occur when satisfying $\omega_L = I_p/n$. At first glance, the energy spectra for the two geometries are similar. With close inspection of the counter-rotating geometry of TDSE, when $\omega_L$ ranges from 0.3 to 0.45 a.u. in the two-photon ionization regime, an exclusive structure appears below the first-order ATI [see the dashed red ellipse in Fig. 2(c)]. In the following, we will show that this feature is directly related to the transition of the circular dichroism. The SFA model does not reproduce this subpeak below the main ATI peak, because it does not include the intermediate states in the interaction. For the corotating case, the SFA result agrees well with the TDSE simulation, indicating that the intermediate states play a minor role in this geometry. Note that the experimental spectrum is the noncoherent sum of the results from $p_+$, $p_{-1}$, and $p_0$ [47]. To observe such photoionization circular dichroism from the neutral atoms presented here, one can first use a pump pulse to break the orbital symmetry of the ground state and then probe the remaining ring current in the ion by another circularly polarized light pulse [20,21].

In order to directly visualize the contribution of different ionization channels, we have performed the calculation of the state-resolved population by projecting the final wave function $\psi(t_f)$ to the eigenstates of the system after the laser turns off when solving the TDSE. This allow us to differentiate the contributions between bound and ionized wave functions and also trace the ionization pathways via different quantum states. For simplicity, here we only use the angular part $|l, m\rangle$ to represent the partial wave function. In Figs. 3(b) and 3(d), we show the extracted population of the final states $|l, m\rangle$ with respect to the laser frequency for the co- and counter-rotating geometries. In those plots, the quantum numbers $l$ and $m$ of the populated states serve as the vertical coordinate. Then we have analyzed the electron transition paths through the related quantum states $|l, m\rangle$ for the two geometries. The selection rule of $l$ is $\Delta l = \pm 1$ and that of $m$ is $\Delta m = 1$ when absorbing each right circularly polarized photon within the dipole approximation. For the corotating geometry, the electron transition path is unique (i.e., $|1, 1\rangle \rightarrow |2, 2\rangle \rightarrow |3, 3\rangle$),
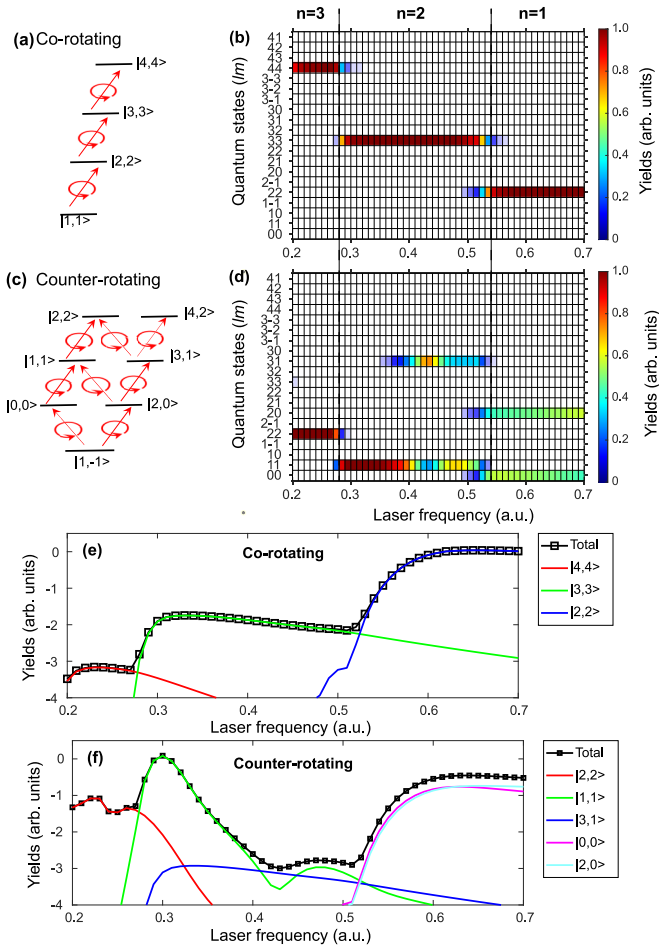
FIG. 3. (a), (c) The schematic of the transition path for the ionization of the co- and counter-rotating orbitals when absorbing a few photons. (b), (d) The electron populations on the final states $|l, m\rangle$ with respect to the laser frequency for the (b) corotating and (d) counter-rotating (d) geometries calculated by solving the TDSE. At each frequency, the population on each state is normalized to the total ionization probability $|\psi(t_f)|^2$. (e), (f) The total ionization probability and the individual contribution of the related states in the co- and counter-rotating geometries, respectively.
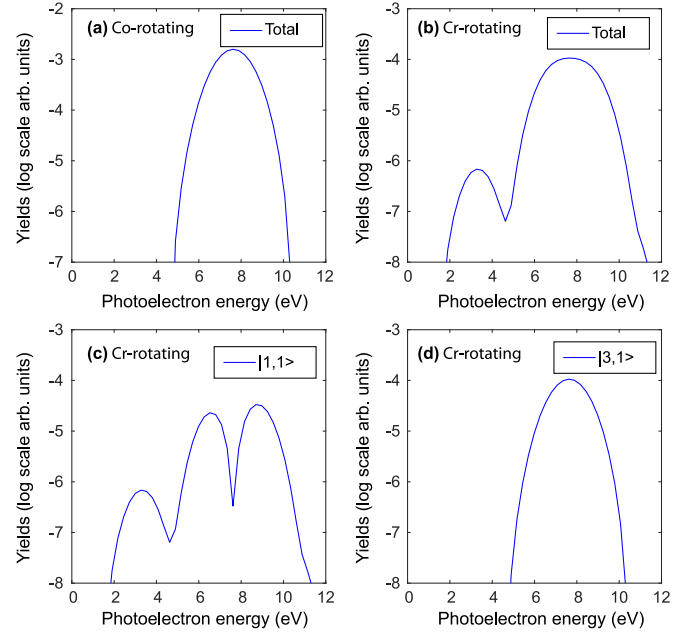


FIG. 4. The photoelectron energy spectra at $\omega_L = 0.43$ a.u. for the ionization of (a) the corotating orbital and (b) the counter-rotating orbital. (c) and (d) are the individual photoelectron energy spectra in the counter-rotating geometry from the states $|1, 1\rangle$ and $|3, 1\rangle$, respectively.

since only the channel of $\Delta l = 1$ can support the select rule of $m$. Our calculation verifies this unique transition path. As illustrated in Figs. 3(b) and 3(e), the larger populated state is $|4, 4\rangle$, $|3, 3\rangle$, $|2, 2\rangle$ for three-photon, two-photon, and single-photon ionization regimes, respectively. Due to the plain ionization mechanism in the corotating case, the SFA result agrees with the TDSE simulation.

As to the counter-rotating geometry, the electron transition path is not unique because the pathways of $\Delta l = 1$ and $\Delta l = -1$ can be both satisfied, as shown in Fig. 3(c). The channel competition will play an important role for the counter-rotating geometry in few-photon ionization. As illustrated in Fig. 3(d), in the three-photon regime the population of $|2, 2\rangle$ is more dominant than that of $|4, 2\rangle$, which indicates the pathway of smaller $l$ is preferred in the multiphoton ionization process. However, in the beginning of the single-photon regime the population of $|2, 0\rangle$ is comparable to that of $|0, 0\rangle$. With an increase of laser frequency the

pathway of larger $l$ becomes more preferred, which is exactly the Fano's propensity rule [53] for single-photon ionization or transition. Therefore, in the two-photon regime the ionization channel through the state of $|1, 1\rangle$ will compete with the ionization channel through $|3, 1\rangle$. Moreover, there are two transition paths ($|1, -1\rangle \rightarrow |0, 0\rangle \rightarrow |1, 1\rangle$ and $|1, -1\rangle \rightarrow |2, 0\rangle \rightarrow |1, 1\rangle$) contributing simultaneously to the state of $|1, 1\rangle$. Thus, it would be expected to have the interference on the state of $|1, 1\rangle$, which depends on the relative phase between those two transition paths. In Fig. 3(f), we show the total ionization probability and the individual contributions from the related states with respect to the laser frequency. The results indicate that the sudden decrease of the total probability originates from the ionization through the state $|1, 1\rangle$. The ionization probability from $|1, 1\rangle$ rapidly drops after entering the two-photon regime and it reaches the minimum at $\omega_L = 0.43$ a.u.. The total probability basically follows the trend of $|1, 1\rangle$.

The interference on the state of $|1, 1\rangle$ takes place in the two-photon regime. The photoelectron energy spectra of those two geometries at $\omega_L = 0.43$ a.u. are shown in Figs. 4(a) and 4(b), respectively. There is a subpeak near the main peak of the ATI in the counter-rotating geometry, whereas the ATI is a single peak in the corotating geometry as only the state $|3, 3\rangle$ is populated. Since the states of $|1, 1\rangle$ and $|3, 1\rangle$ will simultaneously contribute to the total photoelectron energy spectrum of the counter-rotating geometry, we illustrate their individual photoelectron energy spectra in Figs. 4(c) and 4(d). The photoelectron energy spectrum from the state $|3, 1\rangle$ shows a single peak. In contrast, the photoelectron energy spectrum from the state $|1, 1\rangle$ appears as a series of interference peaks because there are two transition pathways involved coherently. Therefore, the subpeak in the counter-rotating ge-
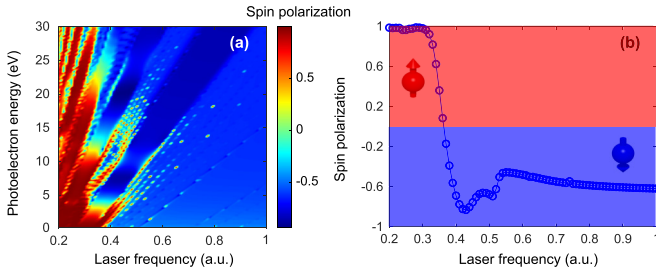
FIG. 5. The energy- and frequency-dependent spin polarization of photoelectrons associated with the ionic state of $j = 1/2$, calculated with the TDSE method. (b) The energy-integrated spin polarization with respect to the laser frequency.

ometry [i.e., the exclusive structure marked by the dashed ellipse in Fig. 2(c)] originates from the channel interference between the transition pathways of $|1, -1\rangle \rightarrow |0, 0\rangle \rightarrow |1, 1\rangle$ and $|1, -1\rangle \rightarrow |2, 0\rangle \rightarrow |1, 1\rangle$. This interference causes the ionization probability to decrease dramatically in the transitional regime and then alters the circular dichroism. Note that here the mechanism of the partial-wave channel interference is the same as the Cooper minimum [54,55].

The natural interest in the photoionization of the ring current is the generation of spin-polarized photoelectrons. Finally, we discuss the photoelectron spin polarization in photoionization with circularly polarized fields. Considering the spin-orbit coupling effect of the ring-current electronic states, the electron spin state could be uniquely related to its orbital state. For example, for the spin-orbit split ionic state of $j = 1/2$ photoelectrons from $p_+$ are spin down and those from $p_-$ are spin up [22–25,27]. Therefore, based on the calculated ionization yields of the $p_+$ and $p_-$ orbitals, we could predict the frequency- and energy-dependent spin polarization of photoelectrons, which is calculated by $S(\omega_L, E_k) = [Y_{up}(\omega_L, E_k) - Y_{down}(\omega_L, E_k)]/[Y_{up}(\omega_L, E_k) + Y_{down}(\omega_L, E_k)]$, where $Y_{up}(\omega_L, E_k)$ and $Y_{down}(\omega_L, E_k)$ are the yields of spin-up and spin-down photoelectrons with the energy of $E_k$ at the driving frequency of $\omega_L$, respectively. In Fig. 5(a), we illustrate the calculated frequency- and energy-dependent spin polarization for the $j = 1/2$ ionic state. In the multiphoton ionization regime, the spin polarization oscillates with the photoelectron energy due to the dichroic energy shift of ATIs. However, in the single-photon regime, the spin polarization is always negative. As illustrated in Fig. 5(b), in the high-frequency limit the energy-integrated spin polarization approaches −0.63. In contrast, the spin polarization could approach 1.0 in the low-frequency limit. The interference process discussed in Fig. 3(f) also plays a noticeable role

in the spin polarization signal. Between 0.4 and 0.5 a.u. frequency, the energy-integrated spin polarization spectrum shows a local peak, which corresponds to the local peak in Fig. 3(f). Note that the two ion channels ($j = 1/2$ and $j = 3/2$) correspond to the different ionization potentials, and thus the photoelectron peak energies are different. Therefore, using a photoelectron energy gate one can separate the contributions from the two channels experimentally. The spin polarizations are opposite between the two ion channels and thus the total spin polarization (i.e., the noncoherent sum of the two channels) will oscillate as a function of photoelectron energy. Several experiments have been performed to explore the spin polarization in multiphoton ionization [23–25]. Resonance-enhanced ionization in the counter-rotating geometry was revealed in Refs. [56–58]. In the intermediate few-photon ionization regime, we show that the spin polarization is determined by the electron dynamics at the doorway states and the spin polarization could change its sign. The results would initiate future interesting experimental explorations of spin-polarized electron generation.

## IV. CONCLUSION

In conclusion, we have investigated the photoionization circular dichroism of electron ring currents of argon atoms from nonadiabatic tunneling ionization to single-photon ionization. Through solving the three-dimensional time-dependent Schrödinger equation, we show that in the two extreme laser-atom-interaction regimes the photoionization circular dichroism and spin polarization obey very different rules, depending on how the frequency of photons matches the rotating speed of the electron ring current. Especially, we show the quantum interference and the competition of the intermediate states with different angular quantum numbers dominate the transition of the circular dichroism in a few-photon ionization regime. This study unifies the pictures of photoionization circular dichroism and spin polarization over a wide range of wavelength, and would have implications for the control of ultrafast circular dichroism of electron ring currents with circularly polarized high-order harmonics sources and x-ray free-electron lasers in the near future.

[1] P. Lambropoulos, Phys. Rev. Lett. **28**, 585 (1972).

[2] R. L. Dubs, S. N. Dixit, and V. McKoy, J. Chem. Phys. **85**, 656 (1986).

[3] M. Ilchen, N. Douguet, T. Mazza, A. J. Rafipoor, C. Callegari, P. Finetti, O. Plekan, K. C. Prince, A. Demidovich, C. Grazioli, L. Avaldi, P. Bolognesi, M. Coreno, M. Di Fraia, M. Devetta, Y. Ovcharenko, S. Düsterer, K. Ueda, K. Bartschat, A. N. Grum-Grzhimailo *et al.*, Phys. Rev. Lett. **118**, 013002 (2017).

[4] J. Hofbrucker, A. V. Volotka, and S. Fritzsche, Phys. Rev. Lett. **121**, 053401 (2018).

[5] N. Böwering, T. Lischke, B. Schmidtke, N. Müller, T. Khalil, and U. Heinzmann, Phys. Rev. Lett. **86**, 1187 (2001).

[6] M. Pitzer, M. Kunitski, A. S. Johnson, T. Jahnke, H. Sann, F. Sturm, L. P. H. Schmidt, H. Schmidt-Böcking, R. Dörner, J. Stohner, J. Kiedrowski, M. Reggelin, S. Marquardt, A. Schießer, R. Berger, and M. S. Schöffler, Science **341**, 1096 (2013).

[7] N. J. Greenfield, Nat. Protoc. **1**, 2876 (2006).

[8] I. Barth and J. Manz, Phys. Rev. A **75**, 012510 (2007).

[9] U. Fano, Phys. Rev. **178**, 131 (1969).

[10] P. Lambropoulos, Phys. Rev. Lett. **30**, 413 (1973).

[11] P. Lambropoulos, J. Phys. B **7**, L33 (1974).

[12] H. A. Bethe and R. W. Jackiw, *Intermediate Quantum Mechanics*, 2nd ed. (W. A. Benjamin, New York, 1968).

[13] K. Rzążewski and B. Piraux, Phys. Rev. A **47**, R1612 (1993).

[14] J. Zakrzewski, D. Delande, J.-C. Gay, and K. Rzążewski, Phys. Rev. A **47**, R2468 (1993).

[15] I. Barth and O. Smirnova, J. Phys. B: At., Mol. Opt. Phys. **47**, 204020 (2014).

[16] I. Barth and M. Lein, J. Phys. B: At., Mol. Opt. Phys. **47**, 204016 (2014).

[17] J. H. Bauer, F. Mota-Furtado, P. F. O'Mahony, B. Piraux, and K. Warda, Phys. Rev. A **90**, 063402 (2014).

[18] M.-M. Liu, M. Li, Y. Shao, M. Han, Q. Gong, and Y. Liu, Phys. Rev. A **96**, 043410 (2017).

[19] S. Eckart, K. Fehre, N. Eicke, A. Hartung, J. Rist, D. Trabert, N. Strenger, A. Pier, L. P. H. Schmidt, T. Jahnke, M. S. Schöffler, M. Lein, M. Kunitski, and R. Dörner, Phys. Rev. Lett. **121**, 163202 (2018).

[20] S. Eckart, M. Kunitski, M. Richter, A. Hartung, J. Rist, F. Trinter, K. Fehre, N. Schlott, K. Henrichs, L. P. H. Schmidt, T. Jahnke, M. S. Schöffler, K. Liu, I. Barth, F. Kaushal, J. Morales, M. Ivanov, O. Smirnova, and R. Dörner, Nat. Phys. **14**, 701 (2018).

[21] T. Herath, L. Yan, S. K. Lee, and W. Li, Phys. Rev. Lett. **109**, 043004 (2012).

[22] I. Barth and O. Smirnova, Phys. Rev. A **88**, 013401 (2013).

[23] A. Hartung, F. Morales, M. Kunitski, K. Henrichs, A. Laucke, M. Richter, T. Jahnke, A. Kalinin, M. Schöffler, L. P. H. Schmidt, M. Ivanov, O. Smirnova, and R. Dörner, Nat. Photonics **10**, 526 (2016).

[24] M.-M. Liu, Y. Shao, M. Han, P. Ge, Y. Deng, C. Wu, Q. Gong, and Y. Liu, Phys. Rev. Lett. **120**, 043201 (2018).

[25] D. Trabert, A. Hartung, S. Eckart, F. Trinter, A. Kalinin, M. Schöffler, L. P. H. Schmidt, T. Jahnke, M. Kunitski, and R. Dörner, Phys. Rev. Lett. **120**, 043202 (2018).

[26] U. Heinzmann and J. H. Dil, J. Phys.: Condens. Matter **24**, 173001 (2012).

[27] M. Han, P. Ge, M.-M. Liu, Q. Gong, and Y. Liu, Phys. Rev. A **99**, 023404 (2019).

[28] O. I. Tolstikhin and T. Morishita, Phys. Rev. A **99**, 063415 (2019).

[29] J. N. Djiokap, S. Hu, L. Madsen, N. Manakov, A. Meremianin, and A. F. Starace, Phys. Rev. Lett. **115**, 113004 (2015).

[30] J. M. Ngoko Djiokap, A. V. Meremianin, N. L. Manakov, S. X. Hu, L. B. Madsen, and A. F. Starace, Phys. Rev. A **94**, 013408 (2016).

[31] D. Pengel, S. Kerbstadt, L. Englert, T. Bayer, and M. Wollenhaupt, Phys. Rev. A **96**, 043426 (2017).

[32] D. Pengel, S. Kerbstadt, D. Johannmeyer, L. Englert, T. Bayer, and M. Wollenhaupt, Phys. Rev. Lett. **118**, 053003 (2017).

[33] J. M. Ngoko Djiokap, A. V. Meremianin, N. L. Manakov, L. B. Madsen, S. X. Hu, and A. F. Starace, Phys. Rev. A **98**, 063407 (2018).

[34] A. De Silva, T. Moon, K. Romans, B. Acharya, S. Dubey, K. Foster, O. Russ, C. Rischbieter, N. Douguet, K. Bartschat *et al.*, Phys. Rev. A **103**, 053125 (2021).

[35] B. Acharya, M. Dodson, S. Dubey, K. Romans, A. De Silva, K. Foster, O. Russ, K. Bartschat, N. Douguet, and D. Fischer, Phys. Rev. A **104**, 053103 (2021).

[36] A. De Silva, D. Atri-Schuller, S. Dubey, B. Acharya, K. Romans, K. Foster, O. Russ, K. Compton, C. Rischbieter, N. Douguet *et al.*, Phys. Rev. Lett. **126**, 023201 (2021).

[37] C. O. Reinhold and C. A. Falcón, Phys. Rev. A **33**, 3859 (1986).

[38] M. Han, P. Ge, Y. Fang, X. Yu, Z. Guo, Y. Deng, Q. Gong, and Y. Liu, Phys. Rev. A **101**, 043406 (2020).

[39] E. Allaria, B. Diviacco, C. Callegari, P. Finetti, B. Mahieu, J. Viefhaus, M. Zangrando, G. De Ninno, G. Lambert, E. Ferrari, J. Buck, M. Ilchen, B. Vodungbo, N. Mahne, C. Svetina, C. Spezzani, S. Di Mitri, G. Penco, M. Trovó, W. M. Fawley *et al.*, Phys. Rev. X **4**, 041040 (2014).

[40] A. Fleischer, O. Kfir, T. Diskin, P. Sidorenko, and O. Cohen, Nat. Photonics **8**, 543 (2014).

[41] A. Ferré, C. Handschin, M. Dumergue, F. Burgy, A. Comby, D. Descamps, B. Fabre, G. A. Garcia, R. Géneaux, L. Merceron, E. Mével, L. Nahon, S. Petit, B. Pons, D. Staedter, S. Weber, T. Ruchon, V. Blanchet, and Y. Mairesse, Nat. Photonics **9**, 93 (2015).

[42] O. Kfir, P. Grychtol, E. Turgut, R. Knut, D. Zusin, D. Popmintchev, T. Popmintchev, H. Nembach, J. M. Shaw, A. Fleischer, H. Kapteyn, M. Murnane, and O. Cohen, Nat. Photonics **9**, 99 (2015).

[43] D. D. Hickstein, F. J. Dollar, P. Grychtol, J. L. Ellis, R. Knut, C. Hernandez-Garcia, D. Zusin, C. Gentry, J. M. Shaw, T. Fan, K. M. Dorney, A. Becker, A. Jaron-Becker, H. C. Kapteyn, M. M. Murnane, and C. G. Durfee, Nat. Photonics **9**, 743 (2015).

[44] P. C. Huang, C. Hernández-García, J. T. Huang, P. Y. Huang, C. H. Lu, L. Rego, D. D. Hickstein, J. L. Ellis, A. Jaron-Becker, A. Becker, S. D. Yang, C. G. Durfee, L. Plaja, H. C. Kapteyn, M. M. Murnane, A. H. Kung, and M. C. Chen, Nat. Photonics **12**, 349 (2018).

[45] K.-Y. Chang, L.-C. Huang, K. Asaga, M.-S. Tsai, L. Rego, P.-C. Huang, H. Mashiko, K. Oguri, C. Hernández-García, and M.-C. Chen, Optica **8**, 484 (2021).

[46] M. Han, J.-b. Ji, K. Ueda, and H. J. Wörner, arXiv:2211.02769.

[47] M. Han, J.-B. Ji, T. Balčiūnas, K. Ueda, and H. J. Wörner, Nat. Phys. **19**, 230 (2023).

[48] V. Mosert and D. Bauer, Comput. Phys. Commun. **207**, 452 (2016).

[49] L. Y. Peng and Q. Gong, Comput. Phys. Commun. **181**, 2098 (2010).

[50] D. B. Milošević, G. G. Paulus, D. Bauer, and W. Becker, J. Phys. B: At., Mol. Opt. Phys. **39**, R203 (2006).

[51] I. Barth and O. Smirnova, Phys. Rev. A **84**, 063415 (2011).

[52] P. Agostini, F. Fabre, G. Mainfray, G. Petite, and N. K. Rahman, Phys. Rev. Lett. **42**, 1127 (1979).

[53] U. Fano, Phys. Rev. A **32**, 617 (1985).

[54] J. W. Cooper, Phys. Rev. **128**, 681 (1962).

[55] M. Y. Amusia, V. Ivanov, N. Cherepkov, and L. Chernysheva, Phys. Lett. A **40**, 361 (1972).

[56] P. Ge, Y. Fang, Z. Guo, X. Ma, X. Yu, M. Han, C. Wu, Q. Gong, and Y. Liu, Phys. Rev. Lett. **126**, 223001 (2021).

[57] S. Walker, L. Kolanz, J. Venzke, and A. Becker, Phys. Rev. A **103**, L061101 (2021).

[58] S. Xu, Q. Zhang, X. Fu, X. Huang, X. Han, M. Li, W. Cao, and P. Lu, Phys. Rev. A **102**, 063128 (2020).